Extended Kalman Filter-Based Gyroscope-Aided Magnetometer Calibration for Consumer Electronic Devices

Ke Han, He Han, Zhifeng Wang, and Feng Xu

***Abstract*— Magnetometers are low-cost sensors that are widely used for orientation sensing in consumer electronic devices. The sensor is affected by non-idealities that can be greatly compensated by proper calibration and determining parameters, such as bias, non-orthogonality, gain, and hard/soft iron. This paper presents a magnetometer calibration method, with the aid of a gyroscope. The algorithm is designed on a principle that the variation of magnetometer output should be aligned with device rotation, which can be sensed by the gyroscope. Based on this notion, an extended Kalman filter is established to estimate calibration parameters. The method evaluation is achieved by first running numerous simulations, followed by a series of experiments on real devices. The result shows that the proposed method can achieve within ten degrees of accuracy, with less than 5 s of convergence. Compared with least square ellipsoid fitting, our proposed method delivers five times better accuracy and avoids over fitting on ill-distributed calibration data sets. This advantage is especially useful for autonomous dynamic calibration in consumer electronic devices.**

***Index Terms*— Magnetometer calibration, gyroscope, extended Kalman filter (EKF), consumer electronics.**

I. Introduction

MAGNETOMETER is widely used in attitude and heading references systems (AHRS), since it can provide both intensity and directional measurement of the Earth's magnetic field. In consumer electronic devices, such as smart phones, tablets, smart glasses, and smart watches, many of them adopt magnetometer(s) in their design, in order to support usages like orientation sensing, gaming control, position navigation, augmented reality, etc. However, due to technological limitations in sensor manufacturing and influence of surrounding ferromagnetic elements, the magnetometer's output data is distorted by various disturbances, and it must be calibrated before use [1].

Many calibration techniques have been presented in literature. Generally, they can be divided into two categories: static calibration with the aid of a certain instrument before application [2]–[7], and dynamic calibration based on existing information from system during application [8]–[17]. Static calibrations usually utilize equipment such as proton magnetometer [2], manual direction placement [3], robot arm [4], Helmholtz coils [5], [6], and turntable [7]. They can achieve better performance, as there are extra reference information from test equipment. However static calibration is only applied in high end devices, since it prolongs the total manufacturing and production time, resulting in a cost adder. Even if the device is calibrated before shipping, dynamic calibration is still needed, as there are usually a lot of magnetized ferromagnetic components on device PCB, and they can be easily affected by external magnetic disturbances. Furthermore, environment temperature change have significant effect on magnetometer readings [8]. In general for consumer electronic devices, it is more practical to have a good dynamic calibration solution.

For dynamic calibration, traditional methods are based on standalone magnetometer sensor, including least square ellipsoid fitting methods [9]–[12], and iterative algorithms [13], [14]. Both algorithms can achieve good calibration results. Ellipsoid fitting methods require proper distribution of data over all directions. Iterative algorithms need large amount of computation and precise initial conditions. For consumer electronic devices, ellipsoid fitting methods usually requires the user to do "figure 8" like gestures, which may not be user friendly, and are not easy to trigger automatically in the background. Recently, there are some new algorithms that are not solely based on magnetometer. Information from inertial sensors [15], integrated navigation system [8], electronic system states [16], environment magnetic field variation [17], and GPS / pitch / roll angle [18] are used in calibration, to bring certain benefits, such as axes alignment calibration, in a fast, autonomous, and accurate manner. However, these solutions all aim at specific usage models such as vehicle [8], aircraft [15], spacecraft [16], and pedestrian navigation [18].

In consumer electronic devices, gyroscope is another commonly used sensor, which outputs angular velocity of the device. In this paper, the relationship between magnetometer and gyroscope is analyzed. Based on this research, an extended Kalman filter (EKF) based gyroscope aided magnetometer calibration algorithm is proposed. The algorithm is designed specifically for consumer electronic devices. As it requires only one additional 3-axis gyroscope along with magnetometer, it can be easily extended into other applications. The key advantage of involving gyroscope into calibration, is to avoid doing the "Figure 8" gesture in today's ellipsoid fitting solutions. With our proposed solution, calibration can be done with daily motions like walking with device, picking up device,

Manuscript received August 23, 2016; revised October 23, 2016; accepted October 25, 2016. Date of publication November 3, 2016; date of current version December 8, 2016. The associate editor coordinating the review of this paper and approving it for publication was Prof. Jürgen Kosel.

The authors are with Intel Asia Pacific Research and Development Ltd., Shanghai 200241, China (e-mail: zjuhank@gmail.com; ke.a.han@intel.com; he.han@intel.com; zhifeng.wang@intel.com; even.xu@intel.com).

Digital Object Identifier 10.1109/JSEN.2016.2624821

1558-1748 © 2016 IEEE. Personal use is permitted, but republication/redistribution requires IEEE permission.
See http://www.ieee.org/publications_standards/publications/rights/index.html for more information.

Authorized licensed use limited to: Zhejiang Lab. Downloaded on May 14,2024 at 02:05:01 UTC from IEEE Xplore. Restrictions apply.

putting down device, etc. The solution described in this paper has been filed as a patent application PCT/CN2014/090817.

This paper consists of the following sections: section II discusses the magnetometer and gyroscope measurement model; section III makes an analysis on the relationship between magnetometer and gyroscope sensor in a rigid body device; section IV shows the model of EKF and specific filtering procedures; last section presents simulation and real device experimental results.

II. Sensor Measurement Model

A. Magnetometer Measurement Model

Magnetometer is sensitive to Earth's magnetic field and any magnetic objects. Generally, a simplified measurement model of magnetometer can be written as

$$\boldsymbol{h}_p = \boldsymbol{A}\boldsymbol{h}_e + \boldsymbol{b}_m + \boldsymbol{\varepsilon}_m \tag{1}$$

In which,

$\boldsymbol{h}_p$ is magnetometer sensor measurement.

$\boldsymbol{A}$ is the rotation matrix of device from Earth Coordinate to Body Coordinate.

$\boldsymbol{h}_e$ is the magnetic field in Earth Coordinate. By definition, it should be [0, by, bz], by and bz can be calculated from test location, from an Earth's magnetic field model.

$\boldsymbol{b}_m$ is the measurement bias of magnetometer sensor, which can be considered as a constant value, if temperature does not change much.

$\boldsymbol{\varepsilon}_m$ is the measurement error of magnetometer sensor. It can be modeled as white noise.

The above proposed model only considers bias and noise. However, in practical usage, there are many other errors, such as sensor scale error, axes non-orthogonality error, and hard / soft iron error caused by surrounding ferromagnetic materials. Considering these factors, a full measurement model [12] can be written as

$$\boldsymbol{h}_p = \boldsymbol{W}\boldsymbol{A}\boldsymbol{h}_e + \boldsymbol{b} + \boldsymbol{\varepsilon}_m \tag{2}$$

In which,

$$\boldsymbol{W} = \boldsymbol{W}_{nonOrth}\boldsymbol{W}_{scale}\boldsymbol{W}_{soft} \tag{3}$$

$$\boldsymbol{b} = \boldsymbol{b}_m + \boldsymbol{b}_{hard} \tag{4}$$

In which,

$\boldsymbol{W}$ is a 3 by 3 matrix, which includes non-orthogonality error matrix $\boldsymbol{W}_{nonOrth}$, gain error matrix $\boldsymbol{W}_{gain}$, and soft iron effect matrix $\boldsymbol{W}_{soft}$. By definition, $\boldsymbol{W}$ is a symmetric matrix.

$\boldsymbol{b}$ is a 3 by 1 vector, which includes bias $\boldsymbol{b}_m$ from sensor, and hard iron effect $\boldsymbol{b}_{hard}$.

$\boldsymbol{W}$ and $\boldsymbol{b}$ are usually considered as constant values, under a given environment. But if there are some big changes in environmental temperature, or in surrounding magnetic environment, parameters like sensor bias, scale error, and hard iron effect can also change. This makes the on-the-fly dynamic calibration important for consumer electronic devices.

With Eq. 2, if $\boldsymbol{W}$ & $\boldsymbol{b}$ are known, it would be easy to get calibrated measurement:

$$\boldsymbol{h}_{cal} = \boldsymbol{A}\boldsymbol{h}_e = \boldsymbol{W}^{-1}\left(\boldsymbol{h}_p - \boldsymbol{b}\right) \tag{5}$$

Notice that noise is preserved in calibrated measurement, which is very common in consumer electronics dynamic calibrations, as removing noise with filters could introduce extra delay in data streaming.

B. Gyroscope Measurement Model

Similar as magnetometer, a full measurement model of gyroscope [19] will be like

$$\tilde{\omega} = \boldsymbol{W}_g\boldsymbol{\omega} + \boldsymbol{b}_{\mathrm{g}} + \boldsymbol{\varepsilon}_{\mathrm{g}} \tag{6a}$$

$$\frac{d\boldsymbol{b}_{\mathrm{g}}}{dt} = \boldsymbol{\varepsilon}_{\mathrm{g-drift}} \tag{6b}$$

$$\boldsymbol{W}_g = \boldsymbol{W}_{g-align}\boldsymbol{W}_{g-nonOrth}\boldsymbol{W}_{g-scale} \tag{6c}$$

In which,

$\boldsymbol{W}_{g-align}$ is the axis alignment error between gyroscope and magnetometer. Because gyroscope and magnetometer are two different sensors, it is possible that axis of both sensors are not strictly aligned. $\boldsymbol{W}_{g-align}$ is a matrix to map gyroscope measurement coordinate to magnetometer measurement coordinate. For high accuracy inertial measurement unit (IMU), this value can be taken into calibration consideration [20].

$\boldsymbol{W}_{g-nonOrth}$ is the non-orthogonality error.

$\boldsymbol{W}_{g-scale}$ is the scale error.

$\boldsymbol{W}_g$ is a combination of above three, and it is not a symmetric matrix.

$\boldsymbol{\varepsilon}_{\mathrm{g}}$ is the measurement noise, it can be modeled as white noise.

$\boldsymbol{b}_{\mathrm{g}}$ is the zero bias, or offset, and it will drift over time. The derivation of drift is modeled by a white noise $\boldsymbol{\varepsilon}_{\mathrm{g-drift}}$.

In this paper, as the algorithm is designed for consumer electronic devices, these systems cannot afford large computations of calibrating gyroscope and magnetometer. So in this paper, a simplified gyroscope model is suggested to be used

$$\tilde{\omega} = \boldsymbol{\omega} + \boldsymbol{\varepsilon}_{\mathrm{g}} \tag{7}$$

In which the gyroscope axis alignment error, non-orthogonality error and scale error are all ignored. In addition, $\boldsymbol{b}_{\mathrm{g}}$ is assumed as a constant value, and it has already been calibrated and removed under tabletop state. Our test results in section V will show that this simplification can be tolerated by EKF algorithm, and will not bring much error in magnetometer calibration.

III. Calibration Principles

A. Constant Magnitude in Magnetic Field

To calibrate a magnetometer, the algorithm needs to rely on several principles that reveal the relationship between magnetometer measurement and trusted references. The most widely used principle is that in the same location, the magnitude of environment magnetic field is constant, regardless the device's orientation [11]. With this principle, we have

$$\boldsymbol{h}_{cal}^T\boldsymbol{h}_{cal} = \left(\boldsymbol{h}_p - \boldsymbol{b}\right)^T\left(\boldsymbol{W}^{-1}\right)^T\boldsymbol{W}^{-1}\left(\boldsymbol{h}_p - \boldsymbol{b}\right) = \text{Constant} \tag{8}$$

The above equation is a general expression defining the locus of the vector $\boldsymbol{h}_p$ lying on the surface of an ellipsoid with center at $\boldsymbol{b}$. It is the fundamental principle in all least square ellipsoid fitting algorithms [9]–[12].

Authorized licensed use limited to: Zhejiang Lab. Downloaded on May 14,2024 at 02:05:01 UTC from IEEE Xplore. Restrictions apply.

B. Alignment Between Magnetometer and Gyroscope

Considering the calibrated magnetometer output in time k and k-1 during rotation

$$\boldsymbol{h}_{cal,k} = \boldsymbol{A}_k \boldsymbol{h}_{\boldsymbol{e}} \tag{10a}$$

$$\boldsymbol{h}_{cal,k-1} = \boldsymbol{A}_{k-1} \boldsymbol{h}_{\boldsymbol{e}} \tag{10b}$$

In which

$\boldsymbol{A}_k$ and $\boldsymbol{A}_{k-1}$ are rotation matrix $\boldsymbol{A}$ at time k and $k-1$.

$\boldsymbol{h}_{cal,k}$ and $\boldsymbol{h}_{cal,k-1}$ are calibrated magnetometer measurement at time k and $k-1$.

Previous solutions utilizes AHRS to obtain rotation matrix [8], [15]. However, this is not applicable for consumer electronic devices, as magnetometer itself is an input in rotation matrix calculation. Unless it is calibrated, there is no way to get accurate attitude measurement.

Nonetheless, though it is hard to get accurate inertial measurement, gyroscope can still be used to aid magnetometer calibration, by the following equation

$$[\boldsymbol{\omega}]_\times = \begin{bmatrix} 0 & -\omega_z & \omega_y \\ \omega_z & 0 & -\omega_x \\ -\omega_y & \omega_x & 0 \end{bmatrix} = \frac{d\boldsymbol{A}}{dt}\boldsymbol{A}^{\mathrm{T}} \tag{11}$$

In which

ω_x, ω_y, ω_z are three axis angular velocity measured by gyroscope.

Eq. 10 can be written as

$$\boldsymbol{A}(t+dt) = \boldsymbol{A}(t) + [\boldsymbol{\omega}(t)]_\times \boldsymbol{A}(t)\,dt \tag{12a}$$

$$\boldsymbol{A}_k = \boldsymbol{A}_{k-1} + \left[\boldsymbol{\omega}_{k-1}\right]_\times \boldsymbol{A}_{k-1}\Delta t \tag{12b}$$

In which, Eq. 11a is the continuous expression, and Eq. 11b is the discrete expression. From Eq. 11a to Eq. 11b, there is some approximation, as Δt is the time interval between time k and k$-$1, which is not a super small value (0.01s in our test).

Multiply $\boldsymbol{b}_{\boldsymbol{e}}$ in both sides of Eq. 11b, then merge Eq. 9a and Eq. 9b to it, the following equation can be derived

$$\boldsymbol{h}_{cal,k} = \left(1 + \left[\boldsymbol{\omega}_{k-1}\right]_\times \Delta t\right) \boldsymbol{h}_{cal,k-1} \tag{13}$$

Eq. 12 reveals the relationship between magnetometer and gyroscope, which is the basis of the proposed EKF calibration solution.

IV. Extended Kalman Filter Based Calibration

In this paper, EKF is proposed to solve the problem, because of the following reasons:

1. EKF is very good at solving non-linear estimation problem in a time varying system

2. For consumer electronics, EKF is more balanced in accuracy and computation, when compared with other non-linear filters like UKF (unscented Kalman filter) and PF (particle filter).

A. State Transition Model

Define EKF state vector as

$$\boldsymbol{x}_k = \left[\boldsymbol{h}_{cal,k}^{T} \;\; W_{11} \;\; W_{22} \;\; W_{33} \;\; W_{12} \;\; W_{13} \;\; W_{23} \;\; \boldsymbol{b}^{\mathrm{T}}\right]^{\mathrm{T}} \tag{14}$$

In which

$W_{11} - W_{33}$ are elements of matrix $\boldsymbol{W}$ in Eq. 2. Since this is a symmetric matrix, only 6 elements are needed to be estimated.

From Eq. 2 and Eq. 12, state transition model $\boldsymbol{x}_k = f(\boldsymbol{x}_{k-1}) + \boldsymbol{W}_{k-1}$ can be written as

$$\boldsymbol{h}_{cal,k} = \left(1 + \left[\boldsymbol{\omega}_{cal,k-1}\right]_\times \Delta t\right) \boldsymbol{h}_{cal,k-1} - \left[\boldsymbol{\varepsilon}_g\right]_\times \Delta t \boldsymbol{h}_{cal,k-1} \tag{15a}$$

$$\boldsymbol{W}_k = \boldsymbol{W}_{k-1} \tag{15b}$$

$$\boldsymbol{b}_k = \boldsymbol{b}_{k-1} \tag{15c}$$

In which,

$\boldsymbol{\omega}_{cal,k-1}$ is the calibrated gyroscope measurement at time k$-$1.

$$\boldsymbol{\omega}_{cal,k-1} = \boldsymbol{\omega}_{k-1} - \boldsymbol{\varepsilon}_g \tag{16}$$

So, the state transition covariance matrix is

$$\boldsymbol{Q}_{k-1} = \begin{bmatrix} \varphi^2 \sigma_g^2 \boldsymbol{h}_{cal,k-1}^{\mathrm{T}} \boldsymbol{h}_{cal,k-1} \Delta t^2 & \boldsymbol{0}_{3\times 9} \\ \boldsymbol{0}_{9\times 3} & \boldsymbol{0}_{9\times 9} \end{bmatrix}. \tag{17}$$

In which

σ_g^2 is the covariance of each element in noise vector $\boldsymbol{\varepsilon}_g$.

φ is a coefficient to compensate the approximation in Eq. 7 and Eq. 11. If gyro is ideal and sampling rate is very high, φ can be set as 1. Otherwise, φ needs to be tuned. φ is an empirical value. In our test cases, 50-300 is a suitable range to handle the non-ideality in industrial grade gyroscope and non-linearity in attitude integration.

As state transition model is linear, its Jacobian matrix can be easily calculated as

$$\boldsymbol{F}_{k-1} = \begin{bmatrix} \left(1 + \left[\boldsymbol{\omega}_{cal,k-1}\right]_\times \Delta t\right) & \boldsymbol{0}_{3\times 9} \\ \boldsymbol{0}_{9\times 3} & \boldsymbol{0}_{9\times 9} \end{bmatrix}. \tag{18}$$

B. Observation Model

From Eq. 2, observation model $\boldsymbol{z}_k = h(\boldsymbol{x}_k) + \boldsymbol{v}_k$ can be written as

$$\boldsymbol{h}_{p,k} = \boldsymbol{W}_k \boldsymbol{h}_{cal,k} + \boldsymbol{b}_k + \boldsymbol{\varepsilon}_m \tag{19}$$

In which

$\boldsymbol{h}_{p,k}$ is the un-calibrated magnetometer measurement at time k.

The measurement covariance matrix is

$$\boldsymbol{R}_k = \sigma_m^2 \boldsymbol{I}_{3\times 3} \tag{20}$$

In which

$$\boldsymbol{h}_k = \left[\boldsymbol{W}_{k|k-1} \;\; \boldsymbol{h}_{Wk} \;\; \boldsymbol{I}_{3\times 3}\right] \tag{9a}$$

$$\boldsymbol{h}_{Wk} = \begin{bmatrix} x_{k|k-1,1} & 0 & 0 & x_{k|k-1,2} & x_{k|k-1,3} & 0 \\ 0 & x_{k|k-1,2} & 0 & x_{k|k-1,1} & 0 & x_{k|k-1,3} \\ 0 & 0 & x_{k|k-1,3} & 0 & x_{k|k-1,1} & x_{k|k-1,2} \end{bmatrix} \tag{9b}$$

Authorized licensed use limited to: Zhejiang Lab. Downloaded on May 14,2024 at 02:05:01 UTC from IEEE Xplore. Restrictions apply.

TABLE I
SIMULATION SETTINGS FOR SCENARIO A

Device rotation	Three axis rotation in sine wave
Sampling freq.	100Hz
Calibration data	Data from first 5 seconds
Test data	Data from 5~60 seconds
Mag magnitude	50 mG
$\boldsymbol{W}$	[1.02 0.02 -0.05 0.02 0.95 -0.03 -0.05 -0.03 1.03]
$\boldsymbol{b}$	$[10 \quad 5 \quad -20]^{\mathrm{T}}$ mG
σ_m	0.5 mG
σ_g	0.1 degree/s$^{1/2}$
$\boldsymbol{x}_0$	$[\boldsymbol{h}_{p,0}\ 1\ 1\ 1\ 0\ 0\ 0\ 0\ 0\ 0]^{\mathrm{T}}$
$\boldsymbol{P}_0$	$[500\boldsymbol{I}_{3\times3} \quad 0 \quad 0$ $0 \quad 10^{-4}\boldsymbol{I}_{6\times6} \quad 0$ $0 \quad 0 \quad 500\boldsymbol{I}_{3\times3}]$
φ	10

TABLE II
SIMULATION SETTINGS FOR SCENARIO B

$\boldsymbol{W}_g$	[1.01 0.03 0.02 0.02 0.97 -0.01 -0.03 -0.01 1.02]
$\boldsymbol{b}_{\mathrm{g}}$	$[0.05 \quad -0.05 \quad 0.1]^{\mathrm{T}}$ degree/s
stdv. of $\boldsymbol{\varepsilon}_{\mathrm{g-drift}}$	0.001 degree/s$^{3/2}$
Other settings	Same as scenario A
φ	100

TABLE III
SIMULATION CALIBRATION RESULT

	Scenario A	Scenario B
$\boldsymbol{W}$	[1.021 0.017 -0.052 0.017 0.950 -0.026 -0.052 -0.026 1.032]	[1.016 0.025 -0.058 0.025 0.948 -0.034 -0.058 -0.034 1.038]
$\boldsymbol{b}$	$[9.92\ 5.06\ -19.84]^{\mathrm{T}}$	$[8.84\ 4.89\ -18.16]^{\mathrm{T}}$
Magnitude	49.99 mG	50.07 mG
RMS	0.53 mG	1.08 mG

σ_m^2 is the covariance of each element in noise vector $\boldsymbol{\varepsilon}_m$.

The observation model is non-linear; its Jacobian matrix can be calculated as

C. EKF Procedures

With linear state transition Eq. 14, and non-linear observation Eq. 16, EKF can be applied to estimate calibrated magnetometer measurement, as well as calibration parameters. Below are the EKF equations:

Predict estimated state and state covariance

$$\boldsymbol{x}_{k|k-1} = f\left(\boldsymbol{x}_{k-1|k-1}\right) \tag{21a}$$

$$\boldsymbol{P}_{k|k-1} = \boldsymbol{F}_{k-1}\boldsymbol{P}_{k-1|k-1}\boldsymbol{F}_{k-1}^{\mathrm{T}} + \boldsymbol{Q}_{k-1} \tag{21b}$$

Update steps

$$\boldsymbol{y}_k = \boldsymbol{z}_k - h\left(\boldsymbol{x}_{k|k-1}\right) \tag{22a}$$

$$\boldsymbol{S}_k = \boldsymbol{h}_k\boldsymbol{P}_{k|k-1}\boldsymbol{h}_k^{\mathrm{T}} + \boldsymbol{R}_k \tag{22b}$$

$$\boldsymbol{K}_k = \boldsymbol{P}_{k|k-1}\boldsymbol{h}_k^{\mathrm{T}}\boldsymbol{S}_k^{-1} \tag{22c}$$

$$\boldsymbol{x}_{k|k} = \boldsymbol{x}_{k|k-1} + \boldsymbol{K}_k\boldsymbol{y}_k \tag{22d}$$

$$\boldsymbol{P}_{k|k} = \left(1 - \boldsymbol{K}_k\boldsymbol{h}_k\right)\boldsymbol{P}_{k|k-1}\boldsymbol{Q}_{k-1} \tag{22e}$$

$\boldsymbol{x}_{k|k}$ and $\boldsymbol{P}_{k|k}$ are the estimated state vector and state covariance matrix on step k.

V. SIMULATION AND REAL SCENARIO TEST RESULTS

A. Simulation Results

To check the effectiveness of proposed EKF solution, a simulation on two scenarios (A and B) is carried out. As discussed in section II.B, one hypothesis in this paper is that gyroscope parameters, such as axis alignment error, non-orthogonality error, and scale error matrix $\boldsymbol{W}_g$ and bias $\boldsymbol{b}_{\mathrm{g}}$, can be ignored. So in scenario A, gyroscope measurement is considered as ideal, and its model follows Eq. 7. In scenario B, gyroscope measurement is considered as non-ideal and its model follows Eq. 6. Table 1 and Table 2 shows the specific settings of both scenarios. These parameters are selected based on measurement of real sensor outputs, and in simulation, gyroscope data are simulated by method introduced in [19]. Furthermore, φ is selected as different value in two tables. This is also because gyro is better in scenario A as its corresponding state transition noise is smaller.

Table 3 shows the simulation calibration results. In this table, the maximum estimation error of scenario A and B for W are 0.004 and 0.008, and maximum estimation error of scenario A and B for b are 0.18 and 1.84 mG. RMS (root mean square) error is defined as the root mean square of distance from calibrated magnetometer measurement to surface of the ideal sphere. In comparison, non-ideal gyroscope measurement in scenario B indeed has some impact on parameters estimation, which will lead to bigger RMS error in calibrated measurement. However, as a bigger φ (100) is selected, and the overall process time is small (5s), this impact is small. 1.08 mG RMS error generally equals to a maximum error of about asin(3∗1.08/50) = 3.72 degree (approximate RMS as std, 3 times std is the maximum error, convert to angle by dividing magnitude and asin), which is still a very good number in consumer electronic device usages.

Fig. 1 and Fig. 2 show the calibration results of calibration data set and test data set in scenario B. The red sphere is the ideal sphere with magnitude 50mG, and the blue dots are calibrated magnetometer measurements with estimated calibration parameters. There are 500 points (5s data) in Fig. 1, and 5,500 points (55s data) in Fig. 2. In these figures, calibrated measurements fit to the ideal sphere pretty well; this also demonstrates the effectiveness of EKF solution.

Fig. 3 and Fig. 4 shows EKF estimation result on element W_{33} and b_x for both Scenario A and Scenario B. As shown, the convergence of EKF is pretty fast; 5s data should be

Authorized licensed use limited to: Zhejiang Lab. Downloaded on May 14,2024 at 02:05:01 UTC from IEEE Xplore. Restrictions apply.

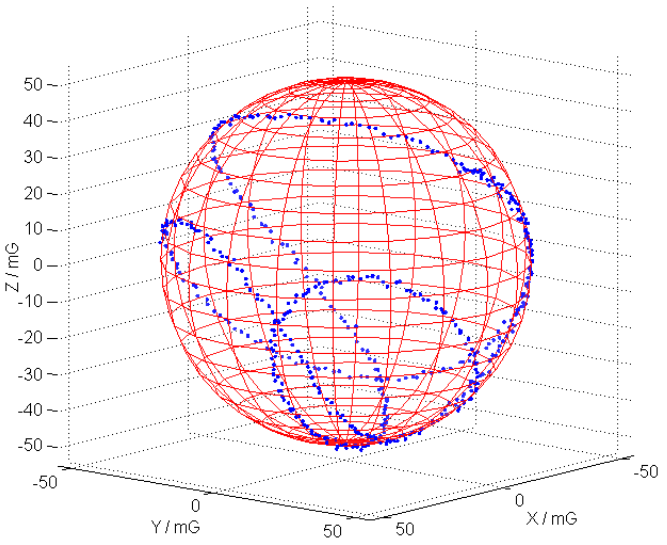

Fig. 1. Calibrated result on calibration dataset (Scenario B).

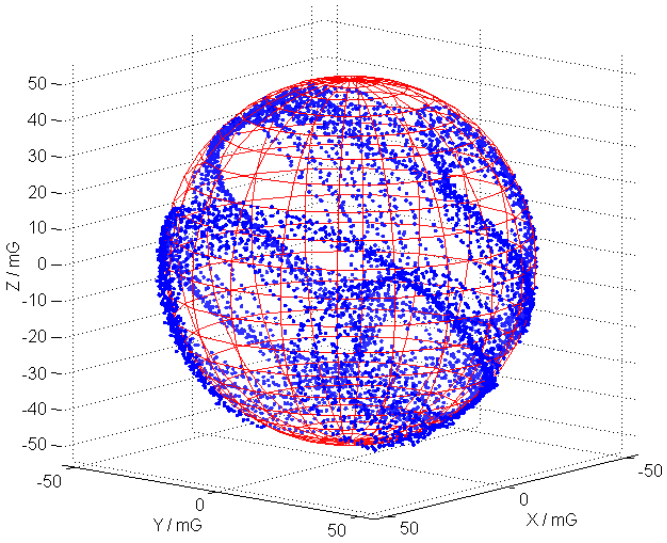

Fig. 2. Calibrated result on test dataset (Scenario B).

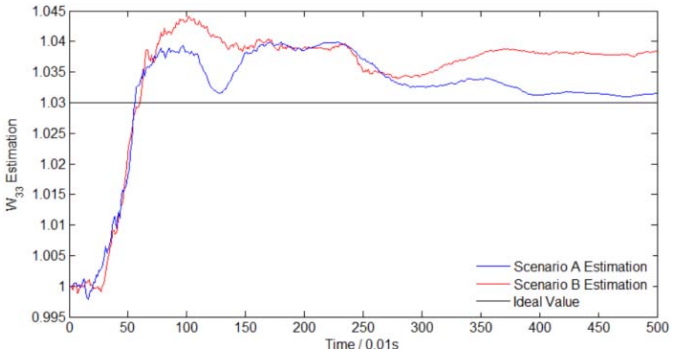

Fig. 3. EKF estimation on W_{33}.

enough to make estimation converge to a stable value. As discussed before, estimation of Scenario B is slightly worse than Scenario A; this is because the model error raised from non-ideal gyroscope measurements. Even through estimation

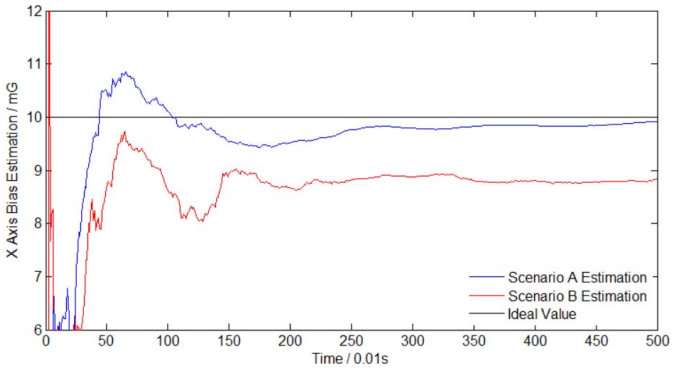

Fig. 4. Estimation on b_x.

TABLE IV
SETTINGS FOR REAL DEVICE TEST

Calibration dataset	9 scenarios from typical daily activities / motions
Evaluation dataset	Collected by "Figure 8" rotation, 20s
Sample freq.	100Hz
σ_m	0.5 mG
σ_g	0.1 degree/s
$\boldsymbol{x}_0$	$[\boldsymbol{B}_{p,k}^{\boldsymbol{T}}\ 1\ 1\ 1\ 0\ 0\ 0\ 0\ 0\ 0]^{\mathrm{T}}$
$\boldsymbol{P}_0$	$[500\boldsymbol{I}_{3\times3}\ \ 0\ \ 0;\ 0\ \ 10^{-4}\boldsymbol{I}_{6\times6}\ \ 0;\ 0\ \ 0\ \ 500\boldsymbol{I}_{3\times3}]$
φ	100

of Scenario A still has some offset to the ideal value, this error is due to the approximation of integration in Eq. 11. Increasing the sampling frequency can reduce such estimation offset.

B. Real Device Test Results

In real device test, an Intel Atom Android phone is used to collect data. Magnetometer and gyroscope sensor chips are LSM303DLHC and L3G4200D from STMicroelectronics. Table 4 listed all the settings in real device test. σ_g and σ_m are parameters in EKF, which are measured before test from test phone. To demonstrate the effectiveness of proposed solution, calibration and evaluation are using separated datasets. In test, evaluation dataset is collected by "Figure 8" rotation, while calibration datasets are collected under 9 different scenarios. Description of these scenarios are listed after Table 4. Except the last scenario (Scenario I), all the other scenarios are typical daily activities / motions from a regular phone user.

Test Scenarios:

A. Walking in a Circle: walking in a circle with device held in hand and swinging beside the leg, pace is 80-100 steps/min, and one circle needs about 23 steps;

B. Walking in a Rectangle: walking in a rectangle with device held in hand and swinging beside the leg, pace is 80-100 steps/min, and one rectangle needs about 19 steps;

C. Walking straight: walking in straight line with device held in hand and swinging beside the leg, pace is 80-100 steps/min;

Authorized licensed use limited to: Zhejiang Lab. Downloaded on May 14,2024 at 02:05:01 UTC from IEEE Xplore. Restrictions apply.

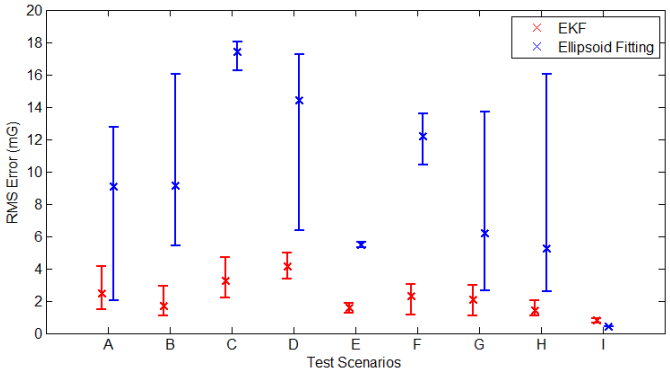

Fig. 5. Comparison test result on real device data.

D. Walking with device in pocket: walking in straight line with device in jacket pocket, pace is 80∼100 steps/min;

E. Device Pickup: pick up phone from pants pocket, hold in front of chest, put back, and repeat, one period lasts about 4s;

F. Place device near ear: hold phone in front of chest, put it near right ear, put back, and repeat, one period lasts about 4s;

G. horizontal rotation: start phone in face up state, rotate it in horizontal plane, one period lasts about 4s;

H. vertical rotation: start phone in portrait state, rotate it in vertical plane, one period lasts about 4.5s;

I. Figure 8 motion: rotate phone in "figure 8" motion, with maximum angular velocity larger than 600 degree/s.

To make the test results more general, data from each above scenario is divided into 10 segments, each last 5s. For scenarios like E∼H, these segments will cover at least one period, with different start and end phases. For scenarios like A∼D, these segments will not cover a full period; instead, data during different phases are tested. In total, there are 90 segments, and EKF is applied on it. After calibration, algorithm performance is calculated by test dataset to measure RMS value.

Besides EKF solution, least square ellipsoid fitting solver was applied for comparison. Ellipsoid fitting is implemented with Matlab function lsqcurvefit, with bound $[-200, 200]$ mG for elements of $\boldsymbol{b}$, $[0.8, 1.2]$ for diagonal elements of $\boldsymbol{W}$, and $[-0.2, 0.2]$ for non-diagonal elements of $\boldsymbol{W}$.

Figure 5 shows the error bar of above 9 scenarios with EKF solution and ellipsoid fitting solution. In Figure 5, ellipsoid fitting is much worse than EKF in almost all scenarios except scenario I (figure 8 motion). It is widely known that ellipsoid fitting method may suffer from overfitting if the calibration dataset is not evenly distributed on all directions. This is exactly the reason why ellipsoid fitting results in poor performance in scenario A∼H. If calibration dataset is distributed ideally on all directions, like scenario I, ellipsoid fitting will be very good, as the RMS error is only 0.4 mG. Table 5 shows the calibration result on this best calibration scenario.

For EKF, the performance is much better as shown by the results in Fig. 5. The key advantage of our proposed solution is that it can work under ill-distributed dataset. This is especially useful for autonomous calibration done in background for consumer electronic devices. Compared with ellipsoid fitting, EKF solution performs much better under user's daily activities, which makes it possible to keep magnetometer sensor always calibrated.

TABLE V
REAL DEVICE CALIBRATION RESULT ON SCENARIO I

	Ellipsoid Fitting	EKF
$\boldsymbol{W}$	[1.008 0.027 -0.017 0.027 0.940 -0.005 -0.017 -0.005 1.057]	[1.012 0.024 -0.031 0.024 0.940 -0.005 -0.031 -0.005 1.051]
$\boldsymbol{b}$	$[-18.86\ 7.38\ -8.02]^T$	$[-18.57\ 7.20\ -7.48]^T$
Magnitude	50.16 mG	50.17 mG
RMS	0.39 mG	0.76 mG

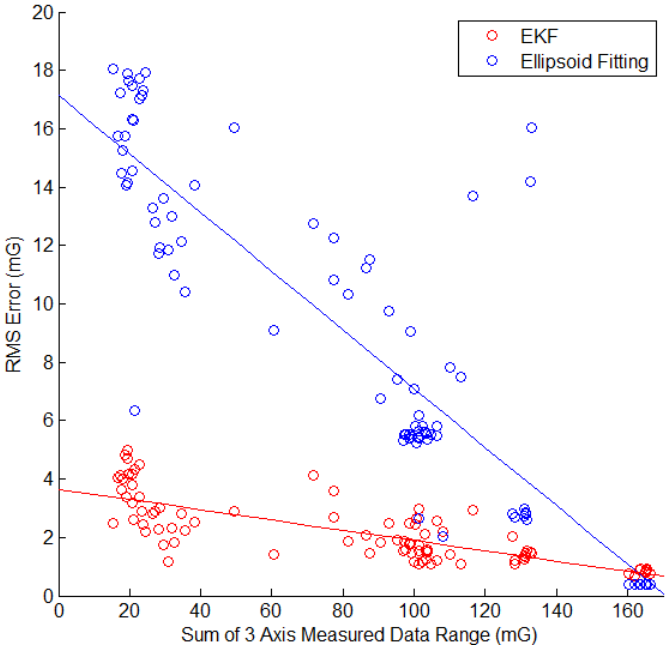

Fig. 6. RMS error vs measured data range.

Compared among different scenarios, it is easy to tell that the more intense activity / motion is, the better RMS value EKF / ellipsoid fitting can achieve. For the most intensive scenario (I. figure 8 motion), EKF RMS error is about 0.8mG from EKF vs 0.4mG from ellipsoid fitting. Such result aligns with previous simulation analysis, the non-optimal calibration is due to non-ideal gyroscope measurement. For less intensive scenarios (A∼H), both ellipsoid fitting and EKF performance are related with the distribution of calibration data, only the severity is different. Fig. 6 shows the relationship of calibration performance (in RMS error) and motion intensity (in sum of 3 axis magnetometer measured data range of 5s). In Fig 6, RMS error generally has a linear relationship with motion intensity, and the slope of EKF is about 5 times smaller than ellipsoid fitting.

With Fig. 6, a method to balance the calibration performance and calibration usability can be derived, by setting a threshold and rejecting less intensive calibration data. For example, if EKF rejects calibration dataset with sum

Authorized licensed use limited to: Zhejiang Lab. Downloaded on May 14,2024 at 02:05:01 UTC from IEEE Xplore. Restrictions apply.

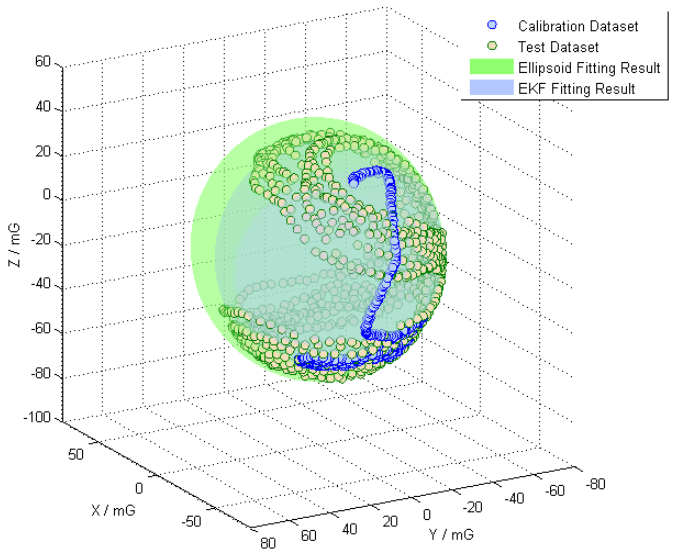

Fig. 7. EKF and ellipsoid fitting on calibration Scenario B (walking in a rectangle).

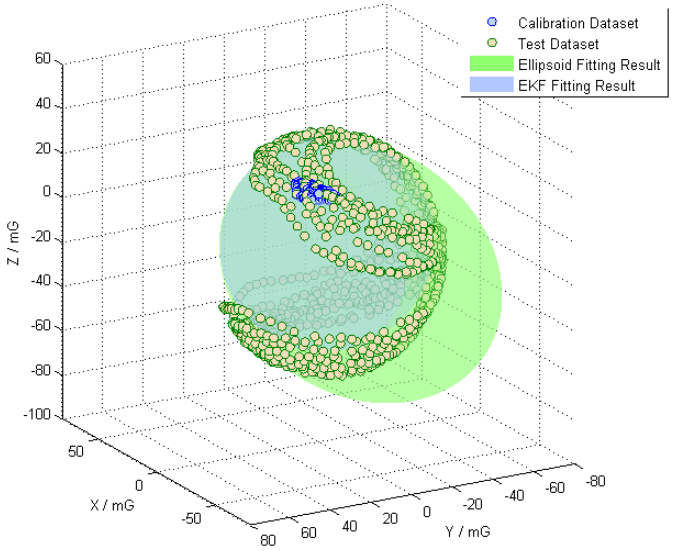

Fig. 8. EKF and ellipsoid fitting on calibration Scenario C (walking straight).

of range below 80 mG, then 36 cases (40%) in test will be rejected. For remaining 54 cases (60%), all cases RMS error are below 3 mG, and 43 cases are below 2 mG.

In specific cases, Fig. 7 and Fig. 8 show the calibration performance on two cases from scenario B and scenario C. Both scenarios are walking cases, only difference is that one has direction change, while the other does not. In Fig. 7, calibration dataset distribute on a larger area than Fig. 8, so both EKF and ellipsoid fitting have better result. RMS of EKF on test dataset in Fig. 7 and Fig. 8 are 1.53 mG and 3.19 mG, while RMS of ellipsoid fitting are 5.57 mG and 17.48 mG. Detailed calibration parameters of Fig. 7 and Fig. 8 are shown in Table 6 and Table 7.

Fig. 9 and Fig. 10 show the calibration performance on two cases from scenario E and scenario G. Although calibration dataset in both cases are distributed widely on surface, data points in Fig. 9 are still ill-distributed, as they are all on one plane, which could easily lead to ellipsoid overfitting.

TABLE VI
RESULT ON CALIBRATION SCENARIO B (RECTANGLE WALKING)

	Ellipsoid Fitting	EKF
$\boldsymbol{W}$	[1.103 -0.041 -0.030 -0.041 0.902 -0.003 -0.030 -0.003 1.007]	[0.995 0.019 -0.014 0.019 0.968 -0.014 -0.014 -0.014 1.039]
$\boldsymbol{b}$	$[-7.29\ 5.19\ -9.16]^{\mathrm{T}}$	$[-21.30\ 7.42\ -7.02]^{\mathrm{T}}$
Magnitude	51.67 mG	50.15 mG
RMS	5.57 mG	1.53 mG

TABLE VII
RESULT ON CALIBRATION SCENARIO C (STRAIGHT WALKING)

	Ellipsoid Fitting	EKF
$\boldsymbol{W}$	[0.872 -0.094 -0.170 -0.094 0.886 0.200 -0.170 0.200 0.878]	[1.012 0.002 -0.011 0.002 0.983 -0.018 -0.011 -0.018 1.005]
$\boldsymbol{b}$	$[-2.42\ 21.76\ -27.59]^{\mathrm{T}}$	$[-19.52\ 7.13\ -3.30]^{\mathrm{T}}$
Magnitude	47.61 mG	50.68 mG
RMS	17.48 mG	3.19 mG

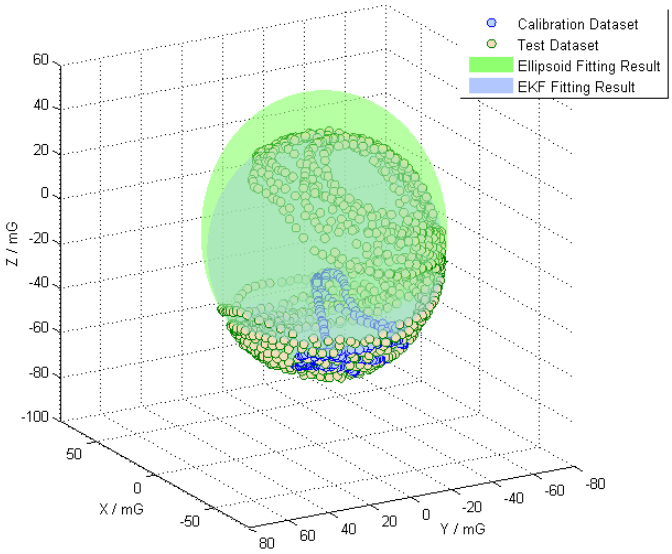

Fig. 9. EKF and ellipsoid fitting on calibration Scenario E (device pickup).

RMS of EKF in both figures are 1.25 mG and 1.56 mG, while RMS of ellipsoid fitting are 5.58 mG and 6.17 mG. Detailed calibration parameters of Fig. 9 and Fig. 10 are shown in Table 8 and Table 9.

In summary, EKF is much better and more robust than ellipsoid fitting in ill-distributed datasets, which commonly happens in daily usages. In test results, EKF's maximum RMS error is within 5mG in all cases. If the use threshold in sum of measured data range rejects less intensive data, then maximum RMS error is within 3mG. 3mG approximately equals to a maximum measurement error of $\mathrm{asin}(3{*}3/50) = 10.37$ degree, which is acceptable for most consumer electronic usages. If user requires higher accuracy, calibration performance can

Authorized licensed use limited to: Zhejiang Lab. Downloaded on May 14,2024 at 02:05:01 UTC from IEEE Xplore. Restrictions apply.

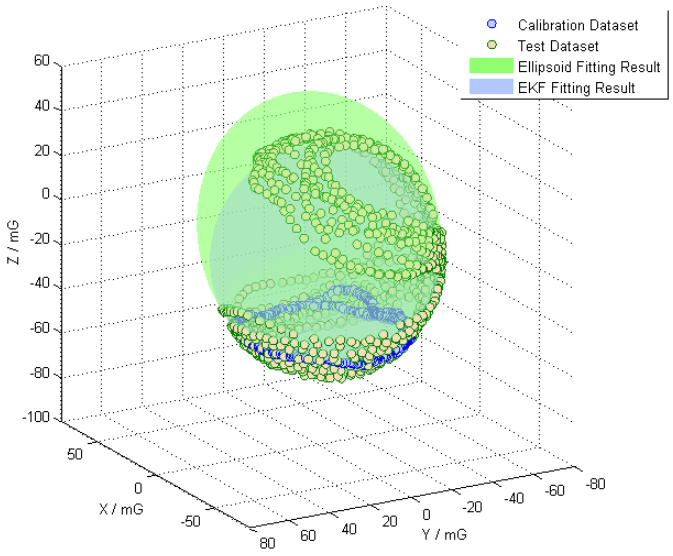

Fig. 10. EKF and ellipsoid fitting on calibration Scenario G (horizontal rotation).

TABLE VIII
RESULT ON CALIBRATION SCENARIO E (PICK UP)

	Ellipsoid Fitting	EKF
$\boldsymbol{W}$	[0.967 0.028 -0.022 0.028 0.912 0.003 -0.022 0.003 1.135]	[0.999 0.027 -0.027 0.027 0.959 0.012 -0.027 0.012 1.044]
$\boldsymbol{b}$	$[-19.29\ \ 8.18\ \ 1.79]^{T}$	$[-20.24\ 7.91\ -6.71]^{T}$
Magnitude	51.09 mG	50.25 mG
RMS	5.58 mG	1.25 mG

TABLE IX
RESULT ON CALIBRATION SCENARIO G (HORIZONTAL ROTATION)

	Ellipsoid Fitting	EKF
$\boldsymbol{W}$	[0.972 0.024 -0.010 0.024 0.907 0.039 -0.010 0.039 1.136]	[1.031 0.025 -0.017 0.025 0.963 -0.012 -0.017 -0.012 1.007]
$\boldsymbol{b}$	$[-18.55\ \ 10.47\ \ 2.05]^{T}$	$[-18.46\ 7.54\ -9.89]^{T}$
Magnitude	51.64 mG	50.29 mG
RMS	6.17 mG	1.56 mG

be further increased by decreasing the threshold. As EKF only needs 5s to converge to an estimation, it is really convenient to run such algorithm in background, and update better calibration parameters from time to time. Compared with traditional calibration methods, proposed EKF solution can bring better user experience, by keeping the magnetometer always calibrated, without any intentional motion input by end user.

VI. CONCLUSION

This paper introduced a novel extended Kalman filter based magnetometer calibration algorithm, with aid of gyroscope data. The principle of this method is based on a fact that magnetometer measurement change should be aligned with rotation of the device, which can be measured with gyroscope. As the algorithm is targeted for consumer electronic devices, some approximation have been made in gyroscope measurement, to simplify the magnetometer & gyroscope alignment model. Based on this model, an extended Kalman filter has been established. The state vector includes calibrated magnetic vector, magnetometer calibration matrix, and magnetometer bias vector.

An evaluation of the proposed extended Kalman filter method is performed using simulation and real device measurements. High accuracy can be achieved after a quick convergence of 5 seconds. The result from extended Kalman filter method is compared with the result obtained by least square ellipsoid fitting. Under ill-distributed dataset, proposed method is five times better in avoiding over fitting and can achieve with 10 degrees of accuracy. This is especially useful for autonomous dynamic calibration in consumer electronic devices, which occurs often in a user's daily life.

REFERENCES

[1] J. Včelák, P. Ripka, A. Platil, J. Kubík, and P. Kašpar "Errors of AMR compass and methods of their compensation," *Sens. Actuators A, Phys.*, vol. 129, nos. 1–2, pp. 53–57, May 2006.
[2] H. F. Pang, S. T. Luo, M. C. Pan, Q. Zhang, and R. F. Xie, "Calibration of three-axis magnetometer diversionary error based on equipment and LMS adaptive algorithm," in *Proc. SPIE*, vol. 7544, P. 75445P, Dec. 2010.
[3] F. Camps, S. Harasse, and A. Monin, "Numerical calibration for 3-axis accelerometers and magnetometers," in *Proc. IEEE Int. Conf. Electro/Inf. Technol.*, Jun. 2009, pp. 217–221.
[4] E. L. Renk, M. Rizzo, W. Collins, F. Lee, and D. S. Bernstein, "Calibrating a triaxial accelerometer-magnetometer—Using robotic actuation for sensor reorientation during data collection," *IEEE Control Syst. Mag.*, vol. 25, no. 6, pp. 86–95, Dec. 2005.
[5] T. Beravs, S. Begus, J. Podobnik, and M. Munih, "Magnetometer calibration using Kalman filter covariance matrix for online estimation of magnetic field orientation," *IEEE Trans. Instrum. Meas.*, vol. 63, no. 8, pp. 2013–2020, Aug. 2014.
[6] A. Zikmund, M. Janosek, M. Ulvr, and J. Kupec, "Precise calibration method for triaxial magnetometers not requiring Earth's field compensation," *IEEE Trans. Instrum. Meas.*, vol. 64, no. 5, pp. 1250–1255, May 2015.
[7] C. H. Ren, Q. Q. Liu, and T. D. Fu, "A novel self-calibration method for MIMU," *IEEE Sensors J.*, vol. 15, no. 10, pp. 5416–5422, Oct. 2015.
[8] A. Wahdan, J. Georgy, W. F. Abdelfatah, and A. Noureldin, "Magnetometer calibration for portable navigation devices in vehicles using a fast and autonomous technique," *IEEE Trans. Intell. Transp. Syst.*, vol. 15, no. 5, pp. 2347–2352, Oct. 2014.
[9] J. Fang, H. Sun, J. Cao, X. Zhang, and Y. Tao, "A novel calibration method of magnetic compass based on ellipsoid fitting," *IEEE Trans. Instrum. Meas.*, vol. 60, no. 6, pp. 2053–2061, Jun. 2011.
[10] W. G. Feng, S. B. Liu, S. W. Liu, and S. L. Yang, "A calibration method of three-axis magnetic sensor based on ellipsoid fitting," *J. Inf. Comput. Sci.*, vol. 10, no. 6, pp. 1551–1558, Apr. 2013.
[11] E. M. Hemerly and F. A. A. Coelho, "Explicit solution for magnetometer calibration," *IEEE Trans. Instrum. Meas.*, vol. 63, no. 8, pp. 2093–2095, Aug. 2014.
[12] Y. Wu and W. Shi, "On calibration of three-axis magnetometer," *IEEE Sensors J.*, vol. 15, no. 11, pp. 6424–6431, Nov. 2015.
[13] H. Yan, C. H. Xiao, S. D. Liu, and Z. Y. Zhang, "Horizontal error calibration method for triaxial fluxgate magnetometer," in *Proc. World Autom. Congr.*, Hawaii, HI, USA, Sep./Oct. 2008, pp. 1–5.
[14] J. F. Vasconcelos, G. Elkaim, C. Silvestre, and P. Oliveira, "A geometric approach to strapdown magnetometer calibration in sensor frame," *IEEE Trans. Aerosp. Electron. Syst.*, vol. 47, no. 2, pp. 1293–1306, Apr. 2011.
[15] M. Kok, J. D. Hol, T. B. Schon, F. Gustafsson, and H. Luinge, "Calibration of a magnetometer in combination with inertial sensors," in *Proc. 15th Int. Conf. Inf. Fusion (FUSION)*, Jul. 2012, pp. 787–793.
[16] K. Han, H. Wang, T. Xiang, and Z. H. Jin, "Magnetometer compensation scheme and experimental results on ZDPS-1A Pico-satellite," *Chin. J. Aeronautics*, vol. 25, no. 3, pp. 430–436, Jun. 2012.

Authorized licensed use limited to: Zhejiang Lab. Downloaded on May 14,2024 at 02:05:01 UTC from IEEE Xplore. Restrictions apply.

[17] J. L. Crassidis, K.-L. Lai, and R. R. Harman, "Real-time attitude-independent three-axis magnetometer calibration," *J. Guid., Control Dyn.*, vol. 28, no. 1, pp. 115–120, 2005.
[18] A. Wahdan, J. Georgy, and A. Noureldin, "Three-dimensional magnetometer calibration with small space coverage for pedestrians," *IEEE Sensors J.*, vol. 15, no. 1, pp. 598–609, Jan. 2015.
[19] J. L. Crassidis, "Sigma-point Kalman filtering for integrated GPS and inertial navigation," in *Proc. Guid., Navigat. Control Conf.*, San Francisco, CA, USA, Aug. 2005.
[20] Y. Wu and S. T. Luo, "On misalignment between magnetometer and inertial sensors," *IEEE Sensors J.*, vol. 16, no. 16, pp. 6288–6297, Aug. 2016.

Ke Han received the B.Sc. and Ph.D. degrees in electronic engineering from the College of Information Science and Electronic Engineering, Zhejiang University, Hangzhou, China, in 2006 and 2011, respectively.

He was with Intel as a Software Engineer from 2011 to 2013 and a Sensor Algorithm Architect from 2014 to 2015. He is currently a Firmware/Software Architect for Intel Integrated Sensor Solution, Intel Asia Pacific Research and Development Ltd. His research interests include sensor calibration, sensor fusion, inertial navigation, and sensor-based context awareness.

He Han received the M.Sc. degree in software engineering from the School of Software Engineering, University of Science and Technology of China, Hefei, China, in 2011.

He has been a Software Developer for Intel Integrated Sensor Solution, Intel Asia Pacific Research and Development Ltd., since 2011. His interests include sensor hub firmware and host software development, sensor calibration, and sensor related power and performance optimization.

Zhifeng Wang received the M.Sc. degree in computer science from the Department of Computer Science and Technology, Tsinghua University, Beijing, China, in 2002.

He is currently managing a team at Intel Asia Pacific Research and Development Ltd., for developing the Intel Integrated Sensor Solution. His interests include sensor firmware/software stack implementation, performance tuning, and power tuning.

Feng Xu received the M.Sc. degree in control theory and control engineering from Hunan University, Changsha, China, in 2007.

He was with Intel as a Firmware Engineer from 2012 to 2013 and an Android Software Engineer from 2013 to 2015. He is currently a Software Driver Engineer for Intel Integrated Sensor Solution, Intel Asia Pacific Research and Development Ltd.

Authorized licensed use limited to: Zhejiang Lab. Downloaded on May 14,2024 at 02:05:01 UTC from IEEE Xplore. Restrictions apply.